NASA TECHNICAL NOTE

NASA TN D-3552

HEAT-TRANSFER ANALYSIS OF THE PLUM BROOK REACTOR

by Harry J. Reilly, Kenneth J. Baumeister, and Salvi Altomare

Lewis Research Center
Cleveland, Ohio

NATIONAL AERONAUTICS AND SPACE ADMINISTRATION • WASHINGTON, D. C. • AUGUST 1966

NASA TN D-3552

HEAT-TRANSFER ANALYSIS OF THE PLUM BROOK REACTOR

By Harry J. Reilly, Kenneth J. Baumeister, and Salvi Altomare

Lewis Research Center
Cleveland, Ohio

NATIONAL AERONAUTICS AND SPACE ADMINISTRATION

For sale by the Clearinghouse for Federal Scientific and Technical Information
Springfield, Virginia 22151 – Price $2.00

HEAT-TRANSFER ANALYSIS OF THE PLUM BROOK REACTOR

by Harry J. Reilly, Kenneth J. Baumeister, and Salvi Altomare

Lewis Research Center

SUMMARY

A heat-transfer analysis of the Plum Brook Reactor (PBR) core was performed to determine fuel-plate surface temperatures, heat fluxes, and the departure-from-nucleate-boiling (DNB) ratio during full power operation. The hot-spot - hot-channel method was employed; the heat-flux distributions in the coolant channels were based on the measured low-power neutron-flux distributions in the cold clean core and in cores containing partially depleted elements.

A statistical method was employed to determine the effects of engineering uncertainties on the reactor heat transfer. The calculations include the effects of asymmetrical cooling of the fuel plates and fuel lumping at the ends of the fuel plates.

A flow coastdown study was performed to determine the required responses of reactor instrumentation following a loss of the main coolant pumps. The calculations were done for the hot spot located by the steady-state analysis.

The results indicate that the analytical methods described give more realistic estimates of the heat-transfer margin during operation at 60 megawatts (thermal) than would be obtained with conventional methods. The observed performance of the reactor indicates that the methods used are sufficiently conservative to ensure the safety of the reactor.

INTRODUCTION

Prior to the start of the work described herein, the Plum Brook Reactor (PBR) construction had been completed, but operation at full power had not begun. Heat-transfer calculations were required to determine the maximum allowable power as a function of control rod position and core loading. An analysis of the heat transfer during flow coastdown was required to determine the appropriate responses of reactor instrumentation.

In performing these calculations, choices had to be made of the techniques to be employed. The conventional hot-spot - hot-channel model was employed for the calculation of nominal conditions. Originally, the conventional direct-multiplier method was used for analysis of engineering uncertainties. Later, the statistical approach shown in this report was adopted. Also, allowance was made for heat conduction in the fuel plates in determining the effects of lumping of the fuel at the ends of the fuel plates and asymmetrical cooling of fuel plates.

The purpose of this report is to describe these calculations with emphasis on those portions of the work that differ from a conventional analysis. The actual performance of the reactor over a 2-year period will be discussed to show that the use of the given methods provided a sufficiently safe operating schedule for the reactor.

CORE DESCRIPTION

The reactor core, which is described in more detail in references 1 and 2, consists of a 3 by 9 array of MTR-type fuel elements, moderated by light water, reflected on all four sides by beryllium elements, and shim-controlled by a bank of five cadmium rods with fueled followers. The coolant water flow is downward through the fueled core, with a total flow of 17 700 gallons per minute. The outlet pressure is set by the head due to a 175-foot elevated tank; the core inlet pressure is about 155 psia and the inlet temperature is less than 135° F during normal operation.

OPERATIONAL CRITERIA

The maximum allowable steady operating power of the PBR is determined by fuel-plate surface temperature and heat-flux limitations provided that the power is not greater than the licensed limit of 60 megawatts (thermal). These limitations have resulted in the choice of certain operating criteria. According to these criteria, the reactor power must be chosen according to the following:

(1) At steady state, the calculated "nominal" fuel-plate surface temperature (i. e., without uncertainty factors) will not exceed the saturation temperature of the coolant.

(2) At steady state, the maximum calculated heat flux will not be greater than one-half of the heat flux which would cause departure from nucleate boiling (DNB).

(3) During a transient condition, the DNB heat flux must be at least 1. 3 times the maximum calculated heat flux. These criteria were adopted prior to full power operation of the PBR and are similar to criteria used by many other water-cooled reactors.

STEADY-STATE HOT-CHANNEL ANALYSIS

Hot-Channel Heat-Transfer Parameters

The analytical approach for nominal conditions was the conventional hot-spot - hot-channel method in which the greatest fuel-plate surface temperatures and heat fluxes in the reactor are calculated and compared with the operating criteria. This requires knowledge of the heat-flux and coolant-flow distributions in the core so that the channel having the limiting performance can be located.

To determine the heat-flux distribution, neutron-flux measurements were performed at several rod bank positions in the uniform core loading and in cores that contained some new elements and some partially depleted fuel elements. The measurements were done with bare and cadmium-covered gold foils and wires and with an automatic semiconductor fission probe device (ref. 1). From the measurements, the detailed three-dimensional power distributions for each bank height and core loading were constructed. The greatest heat fluxes in the core were found to occur at locations adjacent to the beryllium reflectors. Also, the heat-flux distribution is strongly affected by the control rods because the vertical neutron flux peak in the bottom of the core increases as the control rods are inserted.

The coolant-flow distributions were obtained from reference 2. The coolant velocities during normal operation were measured to be 34 fps or greater in channels of nominal 115-mil spacing. Lower velocities existed in some of the channels between fuel-element end plates where manufacturing tolerances can cause below-nominal spacing to occur.

The power distribution data were reduced to a form amenable to digital computation. The heat flux $q(z)$ at elevation z in a channel is expressed as

$$q(z) = \bar{q} F_R F_P F_z \tag{1}$$

(The symbols are defined in appendix A.) Figure 1 shows the hot-channel characteristics for an 18-inch bank position, which is the normal startup position for a 600-megawatt-day cycle (10 days of operation at 60 MW). At an indicated 18 inches, the rod bank is about one-half (12 in.) inserted into the core. As the core depletes, the rods move out and the maximum heat flux decreases; consequently, 18 inches is the worst case for the cycle and is the only case that will be shown herein.

The coolant bulk temperature as a function of vertical position in the hot channel is calculated by a heat balance using the data given in figure 1. The surface temperature $T_w(z)$ is then calculated by

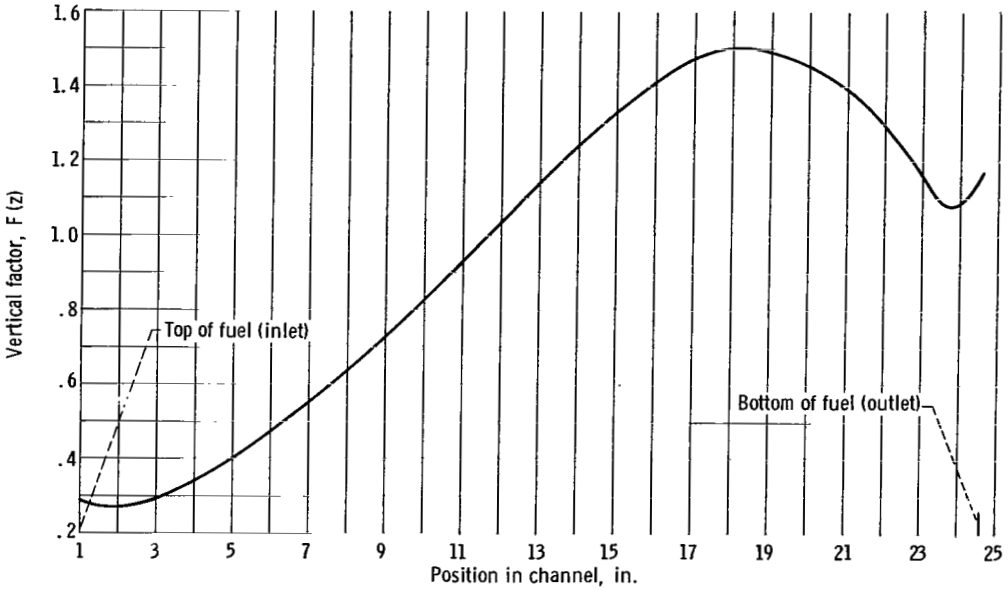

Figure 1. - Hot-channel power distribution. Rods at 18 inches; power, 60 megawatts; radial factor, 1.246; cell factor, 1.171; average coolant velocity, 34 fps; channel spacing, 0.115 inch.

$$T_w(z) = T_b(z) + \frac{q(z)}{h_f} \tag{2}$$

where h_f, as given by the modified Colburn equation (ref. 3), is

$$h_f = 0.023\, Re^{0.8}\, Pr^{0.33}\, \frac{k}{D_e} \tag{3}$$

and the fluid properties are evaluated at the film temperature T_f, which is

$$T_f = \frac{T_w + T_b}{2} \tag{4}$$

A simple device was employed to avoid iteration on the film temperature in the solution of equations (2) and (3). Equation (3) was written as

$$h_f = \frac{K^* V^{0.8}}{D_e^{0.2}} \tag{5}$$

where

$$K^* = 0.023(\rho/\mu)^{0.8}\, Pr^{0.33}\, k \tag{6}$$

For water, K^* is a function of film temperature. Over the temperature range of interest, $150^{\circ}\ F \leq T_f \leq 250^{\circ}\ F$,

$$K^* \doteq 0.1845 + 0.00096\ T_f \tag{7}$$

Substituting equation (7) into equations (5) and (2) and solving for T_w yield

$$T_w(z) = -192.0 + \sqrt{3.68\times10^4 + \frac{2080\ q(z)}{D_e^{-0.2}\ V^{0.8}} + 383\ T_b(z) + T_b(z)^2} \tag{8}$$

The experimental correlations of Bernath (ref. 4) and Mirshak (ref. 5) were used to determine the heat flux at which DNB would occur for comparison with the actual heat flux and with the maximum heat flux including uncertainty factors.

Statistical Approach to Hot-Channel Parameters

In the operation of the PBR, uncertainties exist in dimensions, coolant velocities, flux distributions, and fuel loadings. Variations in these quantities can produce higher surface temperatures and heat fluxes than those calculated by using nominal conditions. It is important to evaluate the combined effects of the uncertainties. Because of their nature, a statistical approach is used. With this approach, a detailed knowledge of the frequency function of the independent variables is required. Reference 6 indicates that these factors may usually be described in terms of a normal error distribution. It is recognized that this may not be true for all the variables and that there is not sufficient information available to choose accurate values for the uncertainties. Therefore, the uncertainty values must be chosen conservatively and the results of the analysis regarded as approximations of the uncertainties in knowledge of the temperatures and heat fluxes.

Evaluation of the uncertainty factors as described in appendix B led to identification of each factor and its variation at a confidence level of 95 percent or greater. The uncertainty factors and their fractional deviations at the 95-percent confidence level are shown in table I. (The functional dependence of the surface temperature and heat flux on these uncertainty factors is discussed in ref. 7. Heat conduction calculations pertaining to the uncertainty factors are shown in appendixes C and D.) The equations used to combine the factors are derived from the relation for the standard deviation of a function that is the product of a number of variables raised to different powers. That is, where $\Gamma = \prod \xi_i^{\alpha_i}$, the ξ_i being independent variables of normal error distribution, and the α_i being constants,

TABLE I. - UNCERTAINTY FACTORS

Parameter	Definition	Fractional deviation at 95-percent confidence, S_{ξ_i}
	Hot channel	
ξ_1	Flux distribution	0.10
ξ_2	Fuel per plate	.05
ξ_3	Coolant velocity measurement accuracy	.03
ξ_4	Velocity distribution among channels	.12
ξ_5	Equivalent diameter	.08
	Hot spot	
ξ_6	Fuel thickness including dogboning	0.15
ξ_7	Channel area at hot spot	.10
ξ_8	Fuel area of plate	.03
ξ_9	Heat-transfer coefficient	.20
ξ_{10}	Fuel core end location	.09
ξ_{11}	Blisters up to 1/8-inch diameter	.15

$$S_\Gamma^2 = \sum_i \left(\frac{\partial \Gamma}{\partial \xi_i}\right)^2 \left(S_{\xi_i}\right)^2 \tag{9}$$

where S_{ξ_i} is the standard deviation in ξ_i. From this the equations for the maximum heat fluxes and temperatures (in terms of the variables in table I) are derived to be

$$q(z)_{max} = q(z)F_q \tag{10}$$

$$T_b(z)_{max} = T_o + \Delta T_b(z)F_b \tag{11}$$

$$T_w(z)_{max} = T_b(z)_{max} + \frac{q(z)}{h_f} F_\theta \tag{12}$$

where

$$F_q = 1 + \sqrt{S_{\xi_1}^2 + S_{\xi_2}^2 + \left(0.8\, S_{\xi_4}\right)^2 + S_{\xi_6}^2 + S_{\xi_8}^2 + S_{\xi_{10}}^2 + S_{\xi_{11}}^2} \tag{13}$$

$$F_b = 1 + \sqrt{S_{\xi_1}^2 + S_{\xi_2}^2 + S_{\xi_3}^2 + \left(S_{\xi_4} + S_{\xi_5}\right)^2} \tag{14}$$

$$F_\theta = 1 + \sqrt{S_{\xi_1}^2 + S_{\xi_2}^2 + \left(0.8\, S_{\xi_3}\right)^2 + \left(0.8\, S_{\xi_4}\right)^2 + S_{\xi_6}^2 + S_{\xi_7}^2 + S_{\xi_8}^2 + S_{\xi_9}^2 + S_{\xi_{10}}^2 + S_{\xi_{11}}^2} \tag{15}$$

where S_{ξ_i} is the relative fractional deviation in ξ_i at the 95-percent confidence level. The resulting values of F_q, F_b, and F_θ are 1.28, 1.23, and 1.36, respectively. That is, there is at least a 95-percent probability that the actual value of q(z) will be within ±28 percent of the nominal value, and there is less than a $2\frac{1}{2}$-percent probability that the heat flux at the hot spot will exceed $q(z)_{max}$ (see eq. (10)).

The uncertainty in the DNB heat flux q_{DNB} was evaluated by differentiating the Mirshak correlation equation

$$q_{DNB} = 479\,000\,(1 + 0.0365\,V)(1 + 0.00507\,T_s)(1 + 0.0131\,P)$$

where

q_{DNB}	DNB heat flux, Btu/(hr)(ft^2)
V	velocity, fps
T_s	subcooling, ^oF
P	pressure, psia

and solving for the relative deviation at the 95-percent confidence level using equation (9) and the data of table I. It was assumed that the accuracy of the correlation for given PBR conditions was ±16 percent at the 95-percent confidence level (ref. 5). The resulting uncertainty in the DNB flux was ±20.7 percent. This led to a value of 0.793 by which the nominal DNB flux must be multiplied to obtain the minimum DNB flux. The nominal and minimum DNB ratios are then calculated by comparing the values of nominal heat flux and DNB flux and by combining the uncertainties on heat flux and DNB flux to obtain

the minimum DNB ratio at the 95-percent confidence level.

RESULTS

Numerical solutions were obtained for the hot-channel heat transfer by using the data of figure 1 (p. 4). The solutions were for a reactor power of 60 megawatts (thermal). The calculated results apply to reactor operation at 60 megawatts; however, for the hot channel the calculations were done for 110-percent normal heat flux because of a possible 10-percent systematic error in reactor power determination. Results are shown in figures 2 to 4: the nominal (most probable) temperatures and heat fluxes are shown along with the maximum values, as defined by equations (10) to (15), and the limiting conditions. The results indicate that the calculated performance is within the operational criteria. Nominal surface temperature does not exceed 280° F, maximum surface temperature does not exceed the saturation temperature, and DNB heat flux is more than twice the maximum heat flux including uncertainty factors.

DISCUSSION

If the uncertainty factors of table I (p. 6) had been combined in the conventional direct-multiplier method, larger overall uncertainties for F_q, F_θ, and F_b would have resulted. Had these values been applied to the calculated nominal temperatures and fluxes - or, as is sometimes done, had only the maximum temperatures and fluxes been

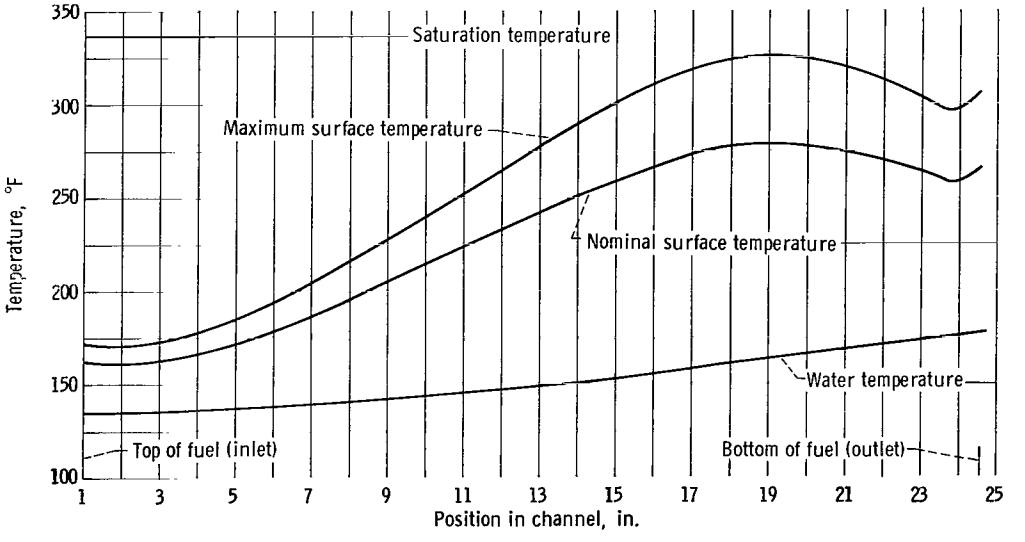

Figure 2. - Hot-channel temperatures. Rods at 18 inches; power, 60 megawatts.

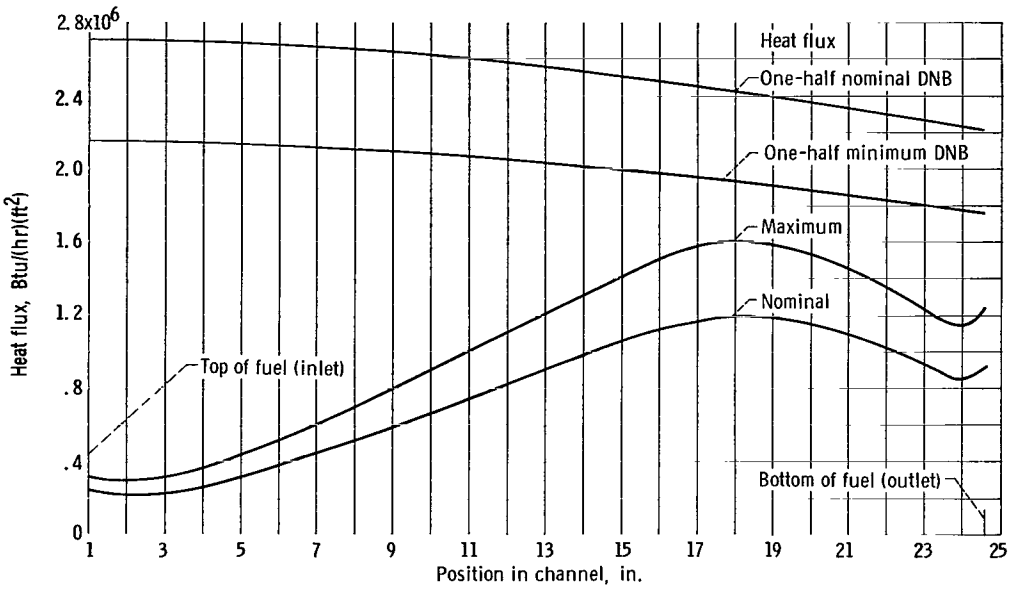

Figure 3. - Hot-channel heat fluxes. Rods at 18 inches; power, 60 megawatts.

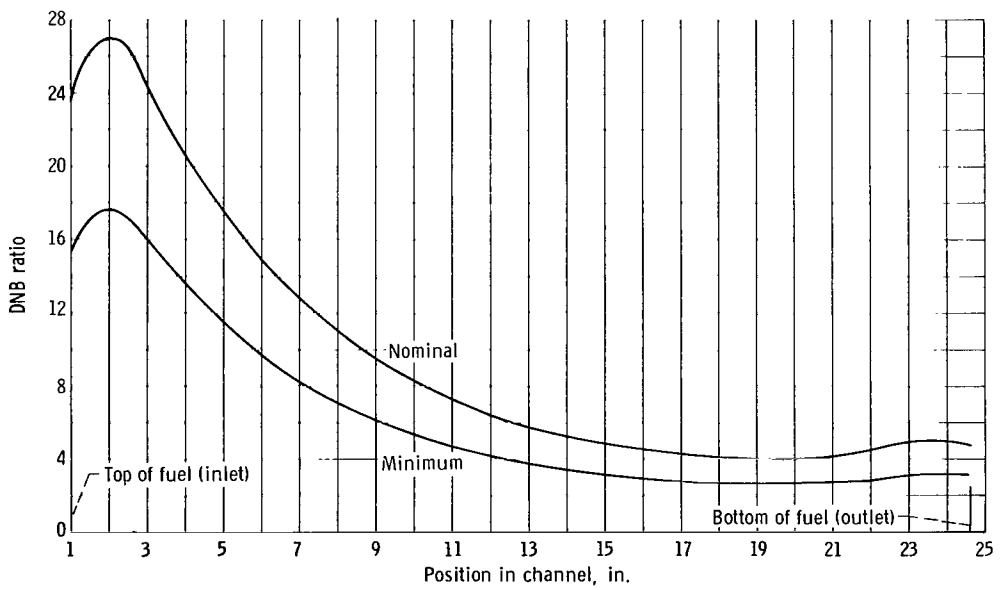

Figure 4. - Hot-channel departure-from-nucleate-boiling (DNB) ratio. Rods at 18 inches, power, 60 megawatts.

calculated - a pessimistic result would have been obtained. The reactor operation at 60 megawatts, rods at 18 inches, would have appeared marginal or a lower power would have been required. The statistical analysis, however, shows the true magnitude of the uncertainties in performance and demonstrates that it is improbable that the reactor will exceed the operating criteria, which themselves are chosen to be conservative.

COOLANT COASTDOWN ANALYSIS

During normal operation the reactor is cooled by two of the three primary pumps and one shutdown pump delivering a total reactor flow of 17 700 gallons per minute. In the event of a loss of both electrical power sources, the coolant flow coasts down, decreasing about 50 percent in the first 2 seconds. The shutdown pump, which uses electrical power generated by diesels, maintains an 1100-gallon-per-minute flow to cool the shutdown core. Because of the rapid coolant coastdown, automatic power reduction actions to protect the core and calculations to determine the required responses were necessary.

Measurements of the flow, pressure, and pressure drop during the coolant coastdown were performed after the low-power tests of reference 1. The behavior of the coolant parameters is shown in figures 5 and 6: the oscillation in the pressures given in figure 6 is assumed to be due to a water-hammer effect of the type described in reference 8.

The scram (automatic reactor shutdown by dropping all shim control rods and safety rods into the core) was assumed to take place with the least favorable conditions (rods out for reactivity worth, but rods at 18 in. for power distribution), and the measured rod bank worths of reference 1 were assumed to apply. The reactivity against time after the start of the scram was described by a sixth-order polynomial, assuming rod drop at a constant acceleration as determined from measurements. The solutions for the flux against time were obtained from a six-group kinetics equation computer program based on the Los Alamos Reactor Transient Solution Code (ref. 9). The gamma decay power was calculated by using the Untermeyer-Weills equation (ref. 10, pp. 7 to 15). The calculated total reactor power against time after scram is shown in figure 7.

Calculations of the surface temperatures and heat fluxes against time were done for the hot spot as determined from the steady-state hot-channel calculations for the 18-inch bank position. The calculations were done assuming the reactor was at a steady-state at each time during the transient. The coolant velocity, bulk temperature, and pressure against time were used to calculate the burnout fluxes during the transient.

Calculations of $T_w(t)$, $q(t)$, and $q_{DNB}(t)$ were done for various scram times. It was decided on the basis of the calculations that scram should occur in no greater than

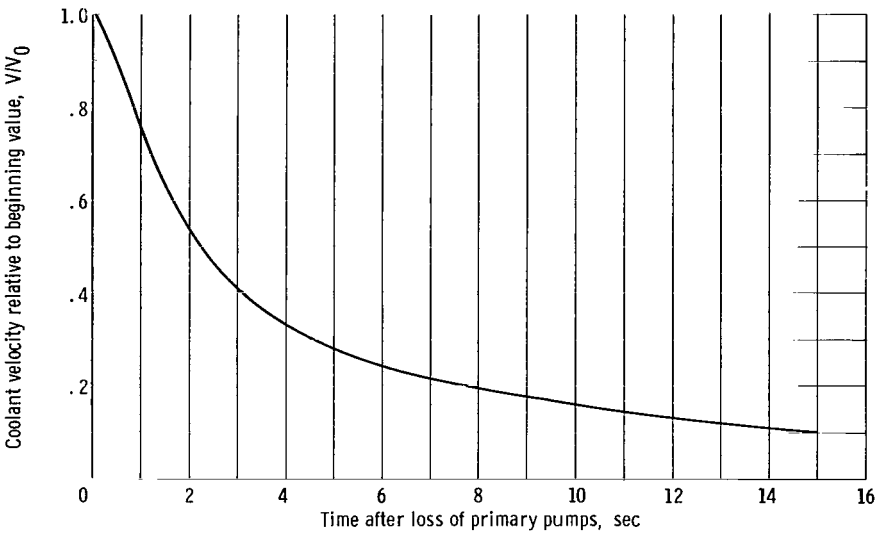

Figure 5. - Coolant velocity ratio after loss of both primary pumps.

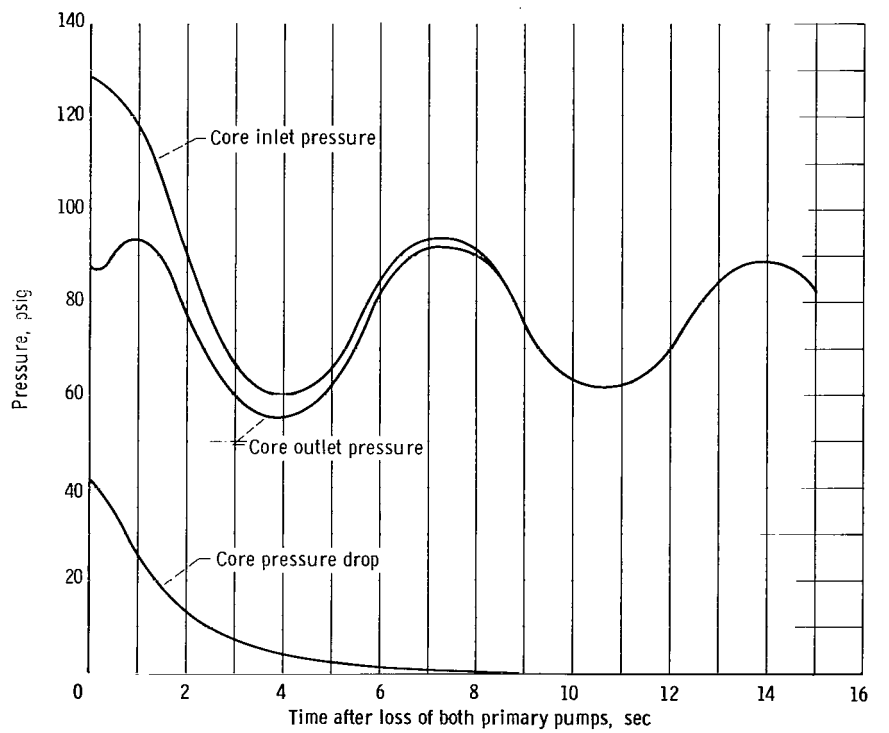

Figure 6. - System pressure after loss of primary coolant pumps.

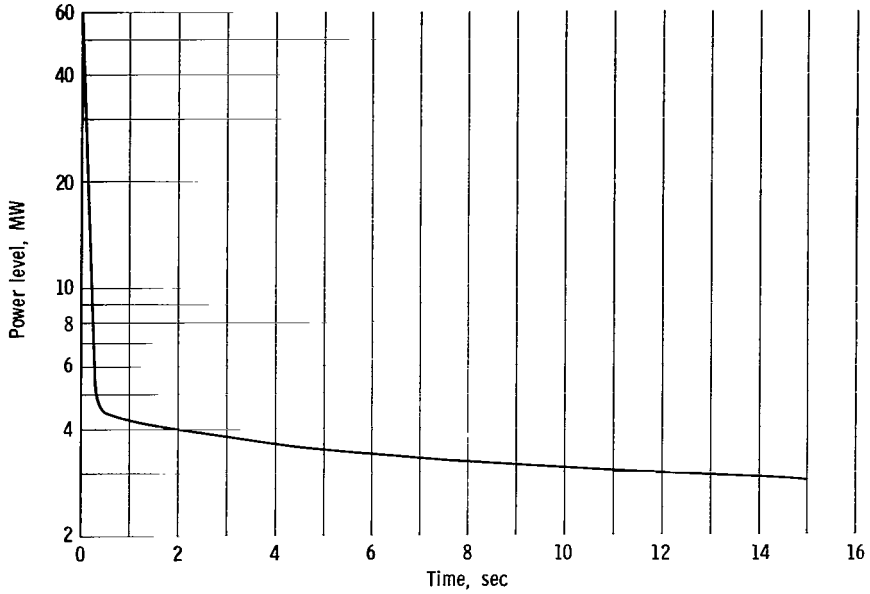

Figure 7. - Reactor power level after rods begin to drop. Full scram, -38 percent reactivity.

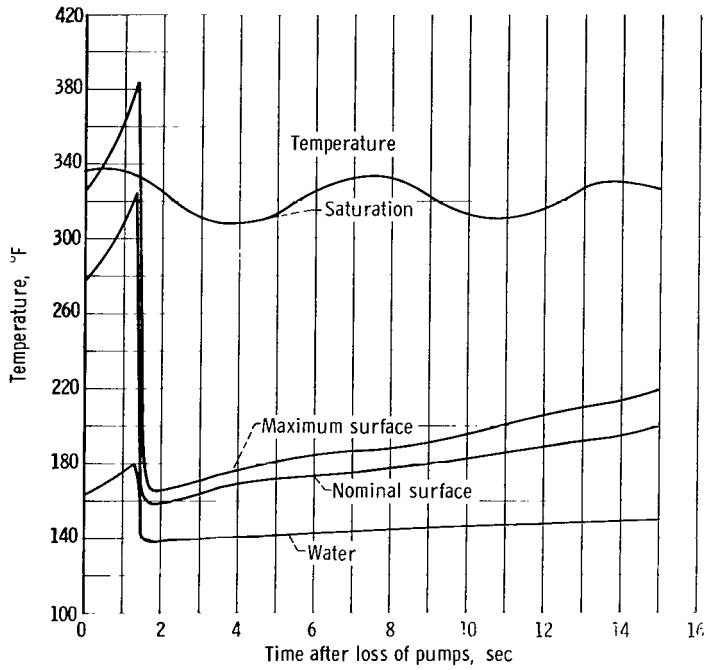

Figure 8. - Temperatures after loss of primary coolant pumps. Full scram at 1.3 seconds.

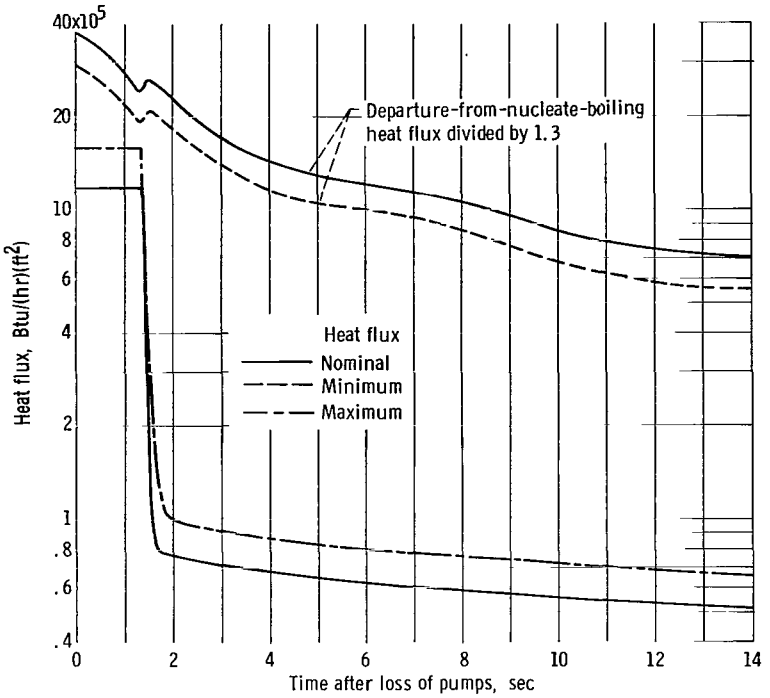

Figure 9. - Heat fluxes after loss of primary coolant pumps. Full scram at 1.3 seconds.

1.3 seconds after loss of pumps. The results of the calculations for this scram time are shown in figures 8 and 9. Nucleate boiling will occur at the hot spot at 1.4 seconds, but the DNB ratio is at least 1.3, which satisfies the operating criterion 3 given on page 2. As a result of the analysis, the reactor inlet pressure and pressure drop instrumentation and the relays monitoring incoming electrical power were set up to guarantee a scram at 1 second after loss of pumps.

Similar calculations were done to determine the required responses for reactor power transients and for other occurrences such as losses in system pressure or temporary interruption of electrical power. In each case, criterion 3 of page 2 was followed. It was determined that (1) a reactor fast scram is required at 1.5 times normal full power, (2) a scram is required at 100 psia, and (3) a loss of one of the two operating primary pumps or an interruption of power from one of the two power sources does not require a reactor scram - a less severe power reduction can be employed.

OPERATING EXPERIENCE

The PBR was first taken critical in June 1961. Measurements of the neutron fluxes and coolant-flow distributions were done in the reactor at low power (refs. 1 and 2). The

reactor operated at high power starting January 1963 and reached design power in April 1963. The reactor had by December 1965 completed 40 cycles at full power, which represents a full-power total operating time of 263 days.

In the first cycle, the reactor was not operated at 60 megawatts until the end of the cycle when only 3 inches of rod travel were left. After cycle 1, the power schedule was adjusted so that the reactor attained 60 megawatts at an indicated 22-inch rod position, which was about half way through the cycle. It was operated in this manner for the first 10 cycles. Then it was decided to use fuel elements in more than 1 cycle so that a given core loading would consist of some new and some used elements at startup. Since cycle 20, operation has been with new and used 200-gram elements beginning with 60-megawatt operation at 18 inches, which is the normal startup position for a 600-megawatt-day cycle. On three separate occasions there were moderate increases in the fission product levels in the primary cooling water. These were caused by excessive uranium 235 contamination of the cladding surfaces or slight cracks or pinhole leaks in the cladding and were not due to failure of heat transfer.

There was one occurrence in which a control system malfunction caused the reactor power to increase on a long period (>10 sec) to 30 percent above normal power followed by a scram. There was no damage to the core from this occurrence.

No instances of observable boiling or solid fission product contamination of the cooling water system have occurred. There was one instance in which a total electrical power failure resulted in a pump coastdown. The reactor scrammed without damage, which indicated that the protective instrumentation functioned satisfactorily and the scram settings were adequate.

CONCLUDING REMARKS

The calculations and the actual operation of the reactor indicate that it is safe to operate at 60 megawatts for the entire cycle beginning with rods at 18 inches. If conventional methods of analysis had been used, such operation would have appeared to be of marginal safety or operation at the start of a cycle might have been restricted to less than 60 megawatts. It is concluded that the methods used, including both the statistical analysis and the conduction calculations, give a more realistic calculational model than the conventional one and allow more efficient operation of the reactor.

Lewis Research Center,
National Aeronautics and Space Administration,
Cleveland, Ohio, April 14, 1966.

APPENDIX A

SYMBOLS

A_s	surface area, ft^2
A_0, A_1	area of channels 0 and 1, ft^2
a	plate thickness, ft
c_p	specific heat capacity of water, Btu/(lb)(^oF)
D_e	equivalent diameter, ft
F_b	combined uncertainty factor on water temperature rise
F_P	cell factor, (heat flux/traverse)/ (heat flux/element)
F_q	combined uncertainty factor on heat flux
F_R	radial factor, (heat flux/element)/$\bar{q}$
F_z	vertical factor, (heat flux at z)/ (heat flux/traverse)
F_θ	combined uncertainty factor on film temperature drop
h_f	heat-transfer coefficient, Btu/(hr)(ft^2)(^oF)
h_0, h_1	heat-transfer coefficient for channels 0 and 1, Btu/(hr)(ft^2)(^oF)
$\bar{h}$	average heat-transfer coefficient, Btu/(hr)(ft^2)(^oF)
K^*	linear fit to the temperature dependent properties of modified Colburn equation over the range $150^o\ F \leq T_f \leq 250^o\ F$
k/ha	dimensionless quantity, conductivity/(heat-transfer coefficient)(thickness)
k	thermal conductivity, Btu/(hr)(ft)(^oF)
L	length of dogbone, in.
ℓ	nominal thickness of fuel core, in.
ℓ'	thickness of dogbone, in.
m	mass flow rate, lb/hr
m_0, m_1	mass flow rate in channels 0 and 1 (half-channel)
Pr	Prandtl number, dimensionless
q(z)	heat flux at elevation z in channel, Btu/(hr)(ft^2)
q_{DNB}	heat flux causing departure from nucleate boiling, Btu/(hr)(ft^2)
q_0, q_1	heat fluxes from surfaces adjacent to channels 0 and 1, Btu/(hr)(ft^2)
$\bar{q}$	average heat flux, Btu/(hr)(ft^2)
q'''	heat generation rate per unit volume, Btu/(hr)(ft^3)
Re	Reynolds number, dimensionless
S_Γ, S_{ξ_i}	standard deviation in quantities Γ and ξ_i
ΔT_b	coolant bulk temperature rise, ^oF

$\overline{\Delta T_b}$	average bulk water temperature rise, ^{o}F
$T_b(z)$	bulk water temperature at elevation z, ^{o}F
$T_{b,0}, T_{b,1}$	bulk water temperature in channels 0 and 1, ^{o}F
T_f	film temperature, ^{o}F
T_o	inlet water temperature, ^{o}F
$T_w(z)$	surface temperature at elevation z, ^{o}F
$T_{w,0'w,1}$	surface temperature adjacent to channels 0 and 1, ^{o}F
V	coolant velocity, ft/hr
V_0, V_1	coolant velocity in channels 0 and 1, ft/hr
x	dimension of solution of equation (D1), through thickness of fuel plate, ft
y	dimension of solution of equation (C8), lengthwise along fuel plate, ft
z	elevation, in.
α_i	coefficients of ξ_i
$\beta(y), \varphi, \psi$	defined on p. 25
Γ	dependent variable defined on p. 5
θ_0	film temperature drop for surface adjacent to channel 0, ^{o}F
$\overline{\theta}$	average film temperature drop, ^{o}F
$\theta_{max}/\theta_{nom}$	ratio of film temperature drop adjacent to dogbone to that without dogbone
μ	coolant viscosity, lb/(hr)(ft)
ξ_i	independent variables, defined in table I
ρ	coolant density, lb/ft^3
τ	width of fuel plate, ft
Ω	volume, ft^3
Subscripts:	
max	maximum value to be experienced
t	denotes function of time
Superscript:	
'	dummy variable

APPENDIX B

DERIVATION OF MAGNITUDES OF UNCERTAINTY FACTORS AT 95-PERCENT CONFIDENCE OR GREATER

Random Uncertainties

Flux distribution - 10 percent. - The 10-percent value was determined by inspection of flux traverse data taken by bare and cadmium-covered gold foils and by an automatic semiconductor fission probe device. Results of one- and two-dimensional computer calculations were examined. It was concluded that the relative flux distributions were accurate to within ±10 percent.

Fuel per plate - 5 percent. - The core loadings consist of fuel elements which when new contain 200 grams of uranium 235 but may have as little as 140 grams at the start of a reactor cycle. The accuracy of the depletion calculation is ±10 percent or 6 grams. This gives about ±5 percent for the uncertainty in the fuel remaining.

Coolant velocity - 3 percent. - A 3-percent value is the accuracy of the turbine flowmeter device used in the hydraulic tests of reference 2.

Velocity distribution and equivalent diameter - 12 and 8 percent. - Analysis and hydraulic tests indicate that the channels between elements can be 0.095 inch thick and have a 26-fps coolant velocity. The analysis of appendix C indicated that a fuel plate cooled by such a channel on one side and a 0.115-inch-thick channel having a 34-fps velocity on the other side is equivalent to a fuel plate cooled by 0.106-inch-thick channels having velocities of 30 fps on each side. These values are 8 and 12 percent less than the nominal 0.115 inch and 34 fps, respectively. (Note that these are not independent variables; also, there is a heat-flux effect as mentioned in appendix C.)

Fuel thickness - 15 percent. - Fuel-core thickness is held to within ±10 percent of nominal in the fabrication procedure. At the fuel core ends (top and bottom), the fuel thickness is limited to give not more than a 15-percent increase in heat flux over nominal as described in appendix C.

Channel area at hot spot - 10 percent. - It is possible for a coolant channel to have nonuniform spacing. If most of the channel is 5 percent below nominal, with a localized spacing of 5 percent above nominal, the effect would be to reduce coolant velocity at the point of larger spacing.

Fuel area - 3 percent. - The fuel area is determined by measurements of fuel-plate radiographs.

Heat-transfer coefficient - 20 percent. - This is the accuracy with which the correla-

tion fits the measured data.

Fuel core end location - 9 percent. - In cases where the hot spot is at the bottom of the core, the variations in location of the fuel core end with respect to the flux traverse become important. The effect of this was determined by measurements of fuel-plate radiographs and measured flux distributions at the bottom reflector flux peak.

Blisters up to 1/8-inch diameter - 15 percent. - The 1/8-inch-diameter blister is the smallest detectable in inspection of new elements. Heat-conduction calculations indicate this would cause a localized increase of 15 percent in the heat flux.

Systematic Uncertainties

Reactor power - 10 percent. - Knowledge of reactor power depends on the accuracy of the water power computer. A study was made of the components of this instrument. The largest error (in the venturi flowmeter) was mostly eliminated by the calibration of this meter during the work of reference 2. The remaining error may tend to be systematic; that is, the instrument is precise but not accurate to better than ±10 percent. This uncertainty factor of 1. 10 was applied as a direct multiplier to the heat-flux data for both nominal and maximum calculations, so that the calculated results apply to reactor operation at a true 66 megawatts (thermal) but are taken to be those for indicated 60 megawatts (thermal).

APPENDIX C

TWO SPECIAL PROBLEMS AND THEIR SOLUTIONS

Asymmetrical Cooling of a Fuel Plate

The conventional practice is to calculate the surface temperature of a fuel plate based on the flow rate in an adjacent channel, assuming half the heat generated in the plate is transferred out each side of the plate. This is accurate when the channels on either side of the plate have the same spacings and coolant velocities such as follows:

When the coolant channels are of different spacings and velocities, the heat fluxes out of the sides of a plate are not equal. Consider the following arrangement:

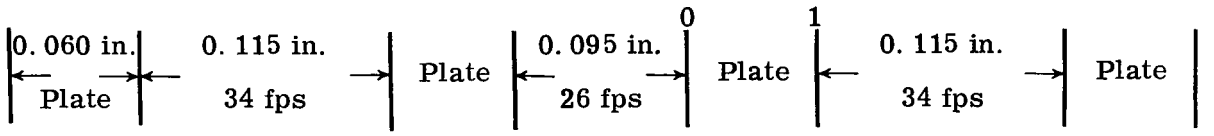

Coolant flow tests in the PBR showed that the coolant velocities in all the 0. 115-inch channels inside the fuel elements were 34 fps; the channels between the fueled end plates had a nominal 0. 120-inch spacing, but were shown to have as little as a 0. 095-inch spacing due to dimensional tolerances and lateral movements of the elements. This resulted in coolant velocities of 26 fps in such channels.

If the conventional practice of assuming half the heat goes into the narrower channel is used, a calculated wall temperature results that is higher than the exact calculated value from a more rigorous approach (see appendix D). Therefore, the numerical heat-transfer code is now adjusted to more accurately account for asymmetrical cooling effects.

Consider the second group of coolant channels: channel 0 represents the small channel with the 26-fps coolant velocity, while channel 1 represents the nominal coolant channel with a 34-fps coolant velocity. It can be assumed for the PBR that $T_{w,0} \cong T_{w,1} \equiv T_w$. This is because the 0. 060-inch-thick aluminum plates in the reactor are so conductive that an asymmetry of the heat fluxes results in a negligible temperature difference. For

the case of interest, $T_{w,0}$ is within 4^{o} F of $T_{w,1}$ when calculated by evaluating equations (D27) and (D28).

Therefore, the calculational model postulated and used to calculate the fuel-plate wall temperature in the coolant channels where asymmetrical heating exists was

$$T_w = T_o + \overline{\Delta T_b} + \bar{\theta} \tag{C1}$$

where

$$\bar{\theta} = \frac{\bar{q}}{\bar{h}} \tag{C2}$$

$$\bar{q} = \frac{q_0 + q_1}{2} \tag{C3}$$

$$\bar{h} = \frac{h_0 + h_1}{2} \tag{C4}$$

$$\overline{\Delta T_b} = \frac{2\int_0^z \bar{q}\, dA_s}{\rho c_p\left(\frac{V_0A_0 + V_1A_1}{2}\right)} \tag{C5}$$

The accuracy of the new calculational model was checked against an analytical solution as given in appendix D. When equation (D11) is used, the ratio of the film drop to that calculated by equation (C2) is

$$\frac{\theta_0}{\bar{\theta}} = \frac{\dfrac{\bar{q}\left(2 + \dfrac{h_1 a}{k}\right) - h_1\left(T_{b,0} - T_{b,1}\right)}{\left(h_0 + h_1 + \dfrac{h_0 h_1 a}{k}\right)}}{\dfrac{\bar{q}}{\left(\dfrac{h_0 + h_1}{2}\right)}} \tag{C6}$$

For the PBR, the percentage error in the film drop was about 1 percent. The error involved in the conventional approach is nearly 10 percent. Similarly, the average bulk temperature defined by equation (C5) was found to agree within 3^{o} F of the exact calcu-

lated value given by equations (D25) and (D26).

The wall temperatures calculated by equation (C1) were compared to the exact solutions and were found to give agreement within $\pm 3^{\circ}$ F. Thus, the uncertainty factor for the below-nominal channel spacing is based on a fuel plate cooled by water at 30 fps in channels of 0.106 inch spacing on either side, rather than 26 fps and 0.095 inch as would be the case for a conventional analysis.

The asymmetric cooling creates a heat flux factor for the plate surface adjacent to the wider channel. That is, the heat flux to the smaller channel is about 10 percent smaller than the average heat flux; the heat flux to the larger or nominal channel (for which the DNB flux is calculated) is 10 percent larger than the average. This factor was included in the calculations and must be borne in mind when comparing the DNB flux with the heat fluxes in figure 3 (p. 9).

Fuel-Element Dogboning

A second problem was nonuniform fuel thickness at the ends of the fuel cores (referred to as dogboning because of its appearance in cross sections of fuel-plate ends). Radiographs of the first fuel elements received indicated that this condition existed. These elements had fuel cores of 16-weight-percent 93-percent-enriched uranium in 1100 aluminum that were fabricated by "picture frame" rolling techniques. Experience with fuel-plate radiographs and sections of fuel plates indicated that the dogbones were less than 1/16-inch long, up to 0.030-inch thick, and irregular over the width of the plate. Inasmuch as this was at the bottom reflector flux peak, the condition appeared to be potentially hazardous.

In order to quantitatively evaluate this problem, the dogboning was represented by the simplified model shown in figure 10. The neutron flux was assumed to be the same

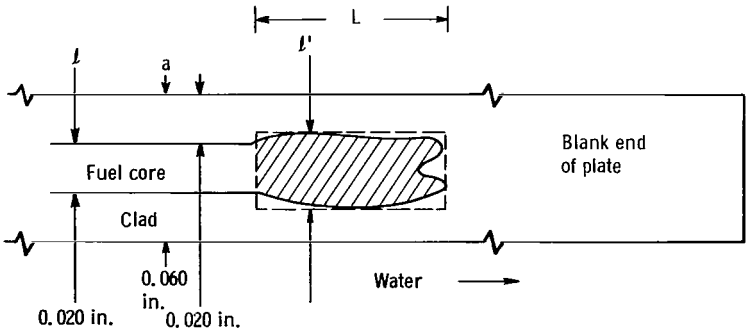

Actual dogboning is shown in cross-hatched area. Dogbone was represented in calculations as being of a rectangular cross section with the same length and maximum thickness as the real dogbone, as shown by the dotted outline.

Figure 10. - Schematic of fuel-core cross section at end of plate.

at all positions. The heat generation was assumed to take place uniformly across the thickness of the plate allowing solution of the steady-state heat-conduction problem in one dimension. The equation

$$-k \frac{d^2T_w}{dy^2} d\Omega + h_f(T_w - T_b)dA = q''' d\Omega \tag{C7}$$

where $d\Omega$ is volume and dA is surface area, for this case reduces to

$$-k \frac{d^2T_w}{dy^2} + \frac{2h_f}{a}(T_w - T_b) = q''' \tag{C8}$$

This equation was set up for numerical solution. Some of the solutions are shown in figure 11. The results for the film temperature drop adjacent to the dogbone are shown in

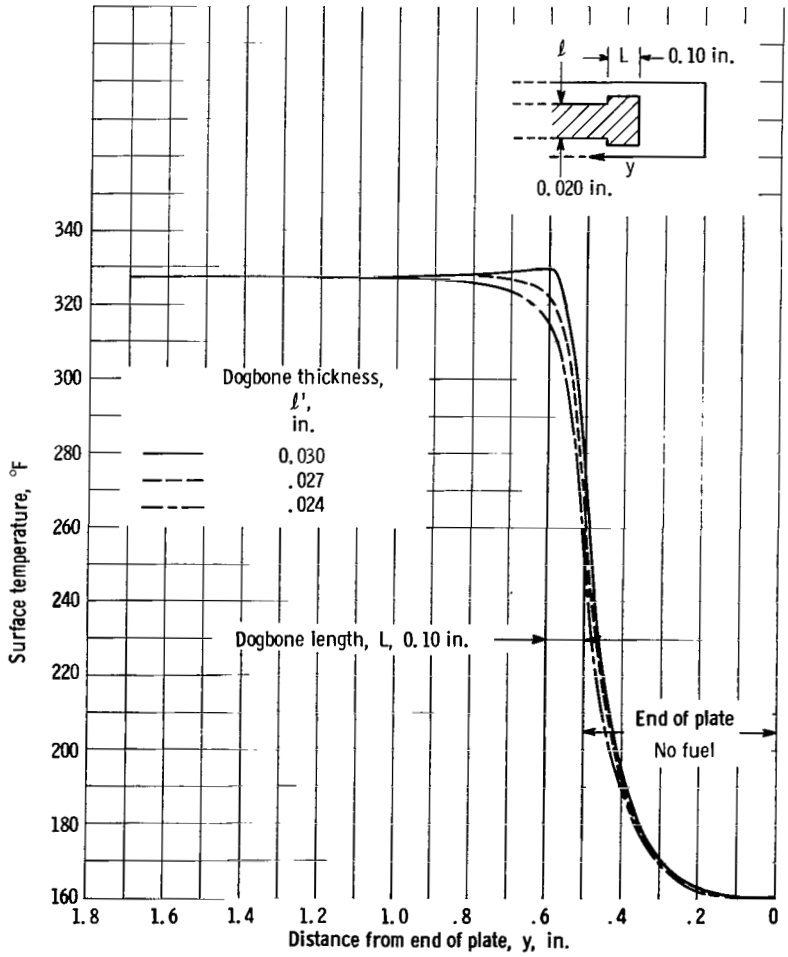

Figure 11. - Surface temperatures near end of fuel plate.

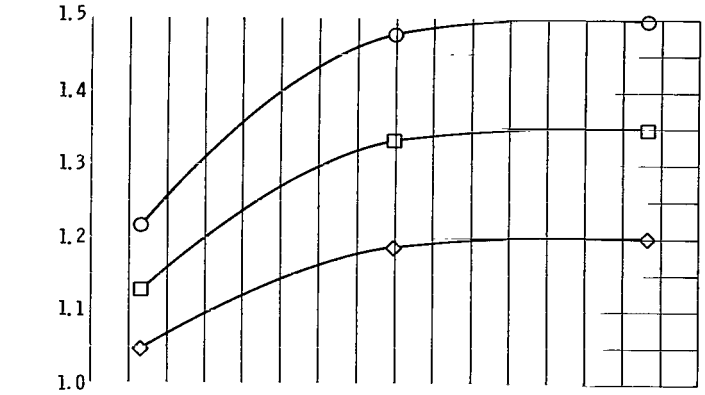

(a) Dimensionless quantity, k/ha, 0.8.

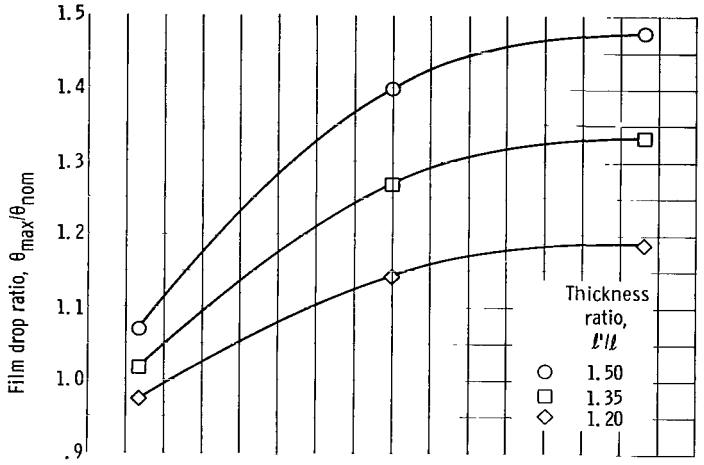

(b) Dimensionless quantity, k/ha, 2.4.

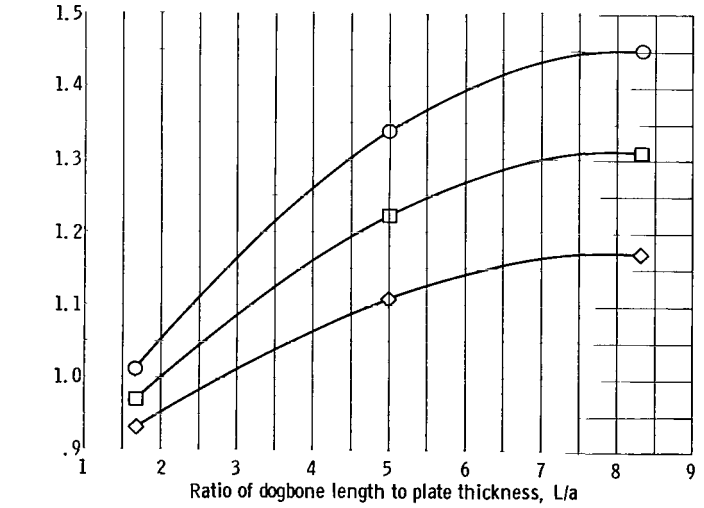

(c) Dimensionless quantity, k/ha, 4.0.

Figure 12. - Dimensionless film temperature drop.

dimensionless form in figure 12. It was decided that a 15-percent increase in the film temperature drop adjacent to the dogbone was the maximum allowable; the use of figure 12 then allowed choice of specifications for fabrication of fuel elements which would meet the given limitations.

APPENDIX D

ANALYTICAL SOLUTION FOR AN ASYMMETRICAL COOLED FLAT PLATE

Consider the problem of a flat-plate fuel element in which the channel spacing and coolant velocities in adjacent channels are unequal, as shown in figure 13. The left coolant channel, designated by 0, is taken to be smaller than the right coolant channel, designated by 1. The 0 and 1 subscripts will be used on the wall and bulk temperatures and any properties of each of the respective channels. The coordinate x represents the position in the fuel element, while the coordinate y represents the axial position in the coolant channel.

The problem is to calculate the wall temperatures, bulk temperatures, and heat fluxes at any point in the channel. To avoid extensive algebra and to keep the mathematics relatively simple, axial conduction in the fuel element is neglected and the internal heat generation is assumed constant across the element. Also, in calculating the bulk temperature rise, an averaged constant heat flux is assumed to exist along the entire length of the channel. Because of the narrowness of the fuel plates, the previous assumptions are acceptable.

The kernel of this problem is to find the temperature distribution in the fuel element and the heat fluxes out each of its faces; thus, the analysis begins by solving Poisson's equation:

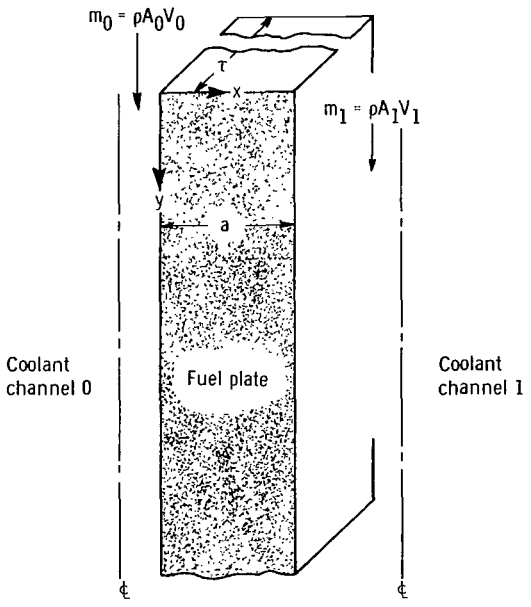

Figure 13. - Schematic of fuel channel.

$$k\frac{d^2T}{dx^2} + q''' = 0 \qquad \text{(D1)}$$

with the boundary conditions

$$T_{w,0} = T_{b,0} - \frac{q_0}{h_0} \qquad \text{(D2)}$$

$$T_{w,1} = T_{b,1} + \frac{q_1}{h_1} \qquad \text{(D3)}$$

It is necessary to use a negative sign in equation (D2), since the heat flux in that direction will be negative in sign.

Solving equation (D1) and applying the boundary conditions (D2) and (D3) yield

$$T(x) = \frac{q'''}{2k}(ax - x^2) + \left(\frac{q_1}{h_1} + \frac{q_0}{h_0}\right)\frac{x}{a} + \frac{\left(T_{b,1} - T_{b,0}\right)x}{a} + T_{b,0} - \frac{q_0}{h_0} \tag{D4}$$

At this time, the internal heat generation rate q''' can be replaced by an average heat flux. Defining

$$q''' \, a \, A_s = 2\bar{q} \, A_s \tag{D5}$$

and substituting into equation (D4) give for the temperature distribution in the fuel plate

$$T(x) = \frac{\bar{q}}{k}\left(x - \frac{x^2}{a}\right) + \left(\frac{q_1}{h_1} + \frac{q_0}{h_0}\right)\frac{x}{a} + \frac{\left(T_{b,1} - T_{b,0}\right)x}{a} + T_{b,0} - \frac{q_0}{h_0} \tag{D6}$$

In equation (D6) the quantities q_0 and q_1 are unknown. However, they can be found by applying Fourier's law

$$q(x) = -k\frac{\partial T}{\partial x} \tag{D7}$$

at the faces of the fuel element. From equation (D6),

$$\frac{\partial T}{\partial x} = \frac{\bar{q}}{k}\left(1 - \frac{2x}{a}\right) + \left(\frac{q_1}{h_1} + \frac{q_0}{h_0}\right)\frac{1}{a} + \frac{\left(T_{b,1} - T_{b,0}\right)}{a} \tag{D8}$$

Evaluating equation (D7) at each of the fuel-element boundaries yields

$$q_0 = -\bar{q} - \frac{kq_1}{h_1 a} - \frac{q_0 k}{h_0 a} + \frac{\left(T_{b,0} - T_{b,1}\right)k}{a} \tag{D9}$$

$$q_1 = +\bar{q} - \frac{kq_1}{h_1 a} - \frac{q_0 k}{h_0 a} + \frac{\left(T_{b,0} - T_{b,1}\right)k}{a} \tag{D10}$$

Solving equations (D9) and (D10) simultaneously for the heat fluxes out the faces of the fuel element yields

$$q_0 = \frac{-\bar{q}\left(2 + \frac{h_1 a}{k}\right) + h_1\left(T_{b,0} - T_{b,1}\right)}{1 + \frac{h_1}{h_0} + \frac{h_1 a}{k}} \tag{D11}$$

$$q_1 = \frac{\bar{q}\left(2 + \frac{h_0 a}{k}\right) + h_0\left(T_{b,0} - T_{b,1}\right)}{1 + \frac{h_0}{h_1} + \frac{h_0 a}{k}} \tag{D12}$$

The heat fluxes out each of the faces of the fuel element can be evaluated from equation (D12) in terms of the heat-transfer coefficients in each channel and the adjacent bulk temperatures. Consequently, the final step in the solution is the determination of the bulk temperatures at any position in the channel.

The bulk temperature at any point in a fuel channel can be expressed simply as

$$T_b(y) = T_o + \frac{1}{mc_p}\int_0^y |q(y)|\tau \, dy \tag{D13}$$

Substituting the values of the heat flux from equations (D11) and (D12) into the previous equation yields

$$T_{b,0} = T_o + \frac{\tau h_0}{m_0 c_p\left(h_0 + h_1 + \frac{h_0 h_1 a}{k}\right)}\left[2\bar{q}\, y + \bar{q}\frac{h_1 a}{k} y - h_1 \int_0^y \left(T_{b,0} - T_{b,1}\right)dy\right] \tag{D14}$$

$$T_{b,1} = T_o + \frac{\tau h_1}{m_1 c_p\left(h_0 + h_1 + \frac{h_0 h_1 a}{k}\right)}\left[2\bar{q}\, y + \bar{q}\frac{h_0 a}{k} y + h_0 \int_0^y \left(T_{b,0} - T_{b,1}\right)dy\right] \tag{D15}$$

The term $\bar{q}$ represents the average heat flux for the channel. If desired, the heat flux distribution as a function of y could have been left under the integral and the exact function form could have been integrated. However, the slight error in the bulk temperatures which results from this assumption has a negligible effect on the wall temperature at the hot spot.

Subtracting equation (D15) from (D14) yields

$$T_{b,0} - T_{b,1} = \frac{\tau}{c_p\left(h_0 + h_1 + \frac{h_0 h_1 a}{k}\right)}\left[2\bar{q}y\left(\frac{h_0}{m_0} - \frac{h_1}{m_1}\right) + \bar{q}y\frac{a}{k}h_0h_1\left(\frac{1}{m_0} - \frac{1}{m_1}\right) - h_1h_0\left(\frac{1}{m_0} + \frac{1}{m_1}\right)\int_0^y \left(T_{b,0} - T_{b,1}\right)dy\right] \quad \text{(D16)}$$

Define

$$\beta(y) \equiv T_{b,0} - T_{b,1} \quad \text{(D17)}$$

$$\varphi \equiv \frac{\tau}{c_p\left(h_0 + h_1 + \frac{h_0 h_1 a}{k}\right)}\left[2\bar{q}\left(\frac{h_0}{m_0} - \frac{h_1}{m_1}\right) + \bar{q}\frac{a}{k}h_0h_1\left(\frac{1}{m_0} - \frac{1}{m_1}\right)\right] \quad \text{(D18)}$$

and

$$\psi \equiv \frac{-\tau h_1h_0\left(\frac{1}{m_0} + \frac{1}{m_1}\right)}{c_p\left(h_0 + h_1 + \frac{h_0 h_1 a}{k}\right)} \quad \text{(D19)}$$

Substituting equations (D17) to (D19) into equation (D16) yields

$$\beta(y) = \varphi y + \psi\int_0^y \beta(y')dy' \quad \text{(D20)}$$

Equation (D20) is a simple integral equation that can readily be solved by reducing it to a differential equation. Differentiating equation (D20) yields

$$\frac{\partial \beta}{\partial y} - \psi\beta = \varphi \tag{D21}$$

From the integral equation, the initial condition for equation (D21) is

$$\left.\begin{aligned} y &= 0 \\ \beta &= 0 \end{aligned}\right\} \tag{D22}$$

The solution for β is

$$\beta = \frac{\varphi}{\psi}\left[\exp(\psi y) - 1\right] \tag{D23}$$

Thus, the bulk fluid temperature difference at any position y is given by

$$T_{b,0} - T_{b,1} = \bar{q}\left[\frac{2\left(1 - \frac{h_1}{h_0}\frac{m_0}{m_1}\right)}{h_1\left(1 + \frac{m_0}{m_1}\right)} + \frac{a\left(1 - \frac{m_0}{m_1}\right)}{k\left(1 + \frac{m_0}{m_1}\right)}\right]\left\{1 - \exp\left[\frac{-\tau h_0\left(1 + \frac{m_0}{m_1}\right)y}{m_0 c_p\left(1 + \frac{h_0}{h_1} + \frac{h_0 a}{k}\right)}\right]\right\} \tag{D24}$$

The term multiplying the exponential term gives the maximum possible deviation in bulk temperature difference if the channel were extended to infinity.

Now, the bulk temperatures at any point in the channel are found by substituting equation (D24) into equations (D14) and (D15). This substitution results in

$$T_{b,0} = T_o + \frac{\tau h_0}{m_0 c_p\left(h_0 + h_1 + \frac{h_0 h_1 a}{k}\right)}\left\{2\bar{q}\,y + \bar{q}\frac{h_1 a}{k}y - h_1\left[\frac{\varphi}{\psi^2}\left(\exp(\psi y) - 1\right) - \frac{\varphi}{\psi}y\right]\right\} \tag{D25}$$

$$T_{b,1} = T_o + \frac{\tau h_1}{m_1 c_p \left(h_0 + h_1 + \frac{h_0 h_1 a}{k}\right)} \left(2\bar{q}\, y + \bar{q}\, \frac{h_0 a}{k}\, y + h_0 \left\{ \frac{\varphi}{\psi^2} \left[\exp(\psi y) - 1 \right] - \frac{\varphi}{\psi} y \right\}\right) \tag{D26}$$

The symbols ψ and φ are defined by equations (D18) and (D19); the values of these symbols in terms of the basic system parameters have not been substituted into the previous expressions in order to keep these equations simpler in form.

The wall temperatures at any point in the channel can now be found by substituting equations (D11) and (D12) into equations (D2) and (D3). This substitution yields

$$T_{w,0} = T_{b,0} + \frac{\bar{q}\left(2 + \frac{h_1 a}{k}\right) - h_1 \left(T_{b,0} - T_{b,1}\right)}{h_0 + h_1 + \frac{h_0 h_1 a}{k}} \tag{D27}$$

$$T_{w,1} = T_{b,1} + \frac{\bar{q}\left(2 + \frac{h_0 a}{k}\right) + h_0 \left(T_{b,0} - T_{b,1}\right)}{h_0 + h_1 + \frac{h_0 h_1 a}{k}} \tag{D28}$$

The bulk temperatures and bulk temperature differences in equations (D27) and (D28) can be found by evaluating equations (D24), (D25), and (D26). Thus, the wall temperatures have been determined explicitly in terms of the system parameters.

REFERENCES

1. Giesler, Harold W.; Reilly, Harry J.; and Poley, William A.: Low-Power Tests of the Plum Brook Reactor. NASA TN D-1560, 1963.

2. Savino, Joseph M.; and Lanzo, Chester D.: Techniques Used to Measure the Hydraulic Characteristics of the NASA Plum Brook Reactor. NASA TN D-1725, 1963.

3. Nertney, R. J., ed.: Calculated Surface Temperatures for Nuclear Systems and Analysis of Their Uncertainties. Rep. No. IDO-16343, Phillips Petroleum Co., June 1957.

4. Bernath, L.: A Theory of Local Boiling Burnout and Its Application to Existing Data. Prepr. No. 110, A.I. Ch. E., Aug. 1959.

5. Mirshak, Samuel; Durant, William S.; and Towell, Robert H.: Heat Flux at Burnout. Rep. No. DP-355, E.I. du Pont de Nemours and Co., Inc., Feb. 1959.

6. Rude, P.A.; and Nelson, A.C., Jr.: Statistical Analysis of Hot Channel Factors. Nucl. Sci. Eng., vol. 7, no. 2, Feb. 1960, pp. 156-161.

7. LeTourneau, B.W.; and Grimble, R.E.: Engineering Hot Channel Factors for Nuclear Reactor Design. Nucl. Sci. Eng., vol. 1, no. 5, Oct. 1956, pp. 359-369.

8. Rich, George R.: Hydraulic Transients. Dover Publications, Inc., 1963.

9. Keepin, G.R.; and Cox, C.W.: General Solution of the Reactor Kinetic Equations. Nucl. Sci. Eng., vol. 8, no. 6, Dec. 1960, pp. 670-690.

10. Etherington, Harold, Ed.: Nuclear Engineering Handbook, McGraw-Hill Book Co., Inc. 1958.

"The aeronautical and space activities of the United States shall be conducted so as to contribute . . . to the expansion of human knowledge of phenomena in the atmosphere and space. The Administration shall provide for the widest practicable and appropriate dissemination of information concerning its activities and the results thereof."

—NATIONAL AERONAUTICS AND SPACE ACT OF 1958

NASA SCIENTIFIC AND TECHNICAL PUBLICATIONS

TECHNICAL REPORTS: Scientific and technical information considered important, complete, and a lasting contribution to existing knowledge.

TECHNICAL NOTES: Information less broad in scope but nevertheless of importance as a contribution to existing knowledge.

TECHNICAL MEMORANDUMS: Information receiving limited distribution because of preliminary data, security classification, or other reasons.

CONTRACTOR REPORTS: Technical information generated in connection with a NASA contract or grant and released under NASA auspices.

TECHNICAL TRANSLATIONS: Information published in a foreign language considered to merit NASA distribution in English.

TECHNICAL REPRINTS: Information derived from NASA activities and initially published in the form of journal articles.

SPECIAL PUBLICATIONS: Information derived from or of value to NASA activities but not necessarily reporting the results of individual NASA-programmed scientific efforts. Publications include conference proceedings, monographs, data compilations, handbooks, sourcebooks, and special bibliographies.

Details on the availability of these publications may be obtained from:

SCIENTIFIC AND TECHNICAL INFORMATION DIVISION

NATIONAL AERONAUTICS AND SPACE ADMINISTRATION

Washington, D.C. 20546